Near-interface electronic and magnetic states of insulator/Co₂MnSi heterostructures probed by hard x-ray photoemission combined with x-ray total reflection

Shigenori Ueda [1,2,*] Yuichi Fujita [3,4,†] and Yuya Sakuraba [3]

[1]*Research Center for Electronic and Optical Materials, National Institute for Materials Science (NIMS), Tsukuba, Ibaraki 305–0044, Japan*
[2]*Synchotron X-ray Station at SPring-8, NIMS, Sayo, Hyogo 679–5148, Japan*
[3]*Research Center for Magnetic and Spintronic Materials, NIMS, Tsukuba, Ibaraki 305–0047, Japan*
[4]*International Center for Young Scientists, NIMS, Tsukuba, Ibaraki 305–0047, Japan*

Depth-dependent electronic and magnetic states of AlO_x and MgO capped Co_2MnSi thin films were measured by using hard x-ray photoemission spectroscopy (HAXPES) combined with x-ray total reflection (TR). TR-HAXPES revealed that the near-interface electronic and magnetic states of Co_2MnSi films differed from those of bulk measured in non-TR condition. The decrease of the Co and Mn magnetizations near the interface along the easy magnetization axis in the bulk region relative to those in the bulk region and the changes in the valence band profiles were experimentally detected by nondestructive HAXPES utilizing TR. The possible origin of the reduction of the Co and Mn magnetizations and the changes in the valence band profile near the AlO_x/Co_2MnSi interface was due to an enhanced spin-wave excitation originating from the weakened exchange interaction between the local magnetic moments compared to the bulk region of Co_2MnSi, which can slightly modify the valence band electronic states, near the interface at a finite temperature. These results suggest that the combination of HAXPES with TR is useful to experimentally detect the electronic and magnetic states of near-interface and buried bulk regions in nondestructive way for insulator/ferromagnet heterojunctions.

I. INTRODUCTION

Half-metallic ferromagnets, in which one spin state exhibits a metallic behavior and the other state exhibits an insulating behavior, are useful for spintronic device applications [1], because the perfect spin polarization (SP, 100%) at the Fermi-level (E_F) is realized. One of potential spintronic applications is magnetoresistance (MR) devices using tunnel and giant MR (TMR and GMR) junctions, in which the half-metals are used for magnetic electrodes, since huge MR ratios are expected due to the perfect SP at E_F in the half-metals. However, the performances of TMR and GMR junctions show a strong reduction with increasing temperature, even though the predicted half-metals such as $L2_1$-ordered Co-based Heusler alloys (Co_2YZ) with high Curie temperature (T_C) sufficiently above room temperature (RT) are used as a magnetic electrode. For example, the $Co_2MnSi(CMS)$/MgO/CMS TMR junction [2] showed the TMR ratios of 2010% at 4.2 K and 335% at RT, and the $Co_2FeGa_{0.5}Ge_{0.5}$/Ag/$Co_2FeGa_{0.5}Ge_{0.5}$ GMR junction [3]

showed the current-perpendicular-to-plane GMR ratios of 285% at 10 K and 82% at RT. The strong reduction in TMR and GMR ratios with increasing temperature is a long-standing issue to be solved.

Jourdan *et al.* [4] reported that an epitaxial CMS(001) thin film showed a high SP of ∼93% at RT by means of a surface-sensitive spin-resolved photoelectron spectroscopy (PES). However, the temperature-dependent SP has not been reported in their work. Recently, a bulk-sensitive spin-resolved hard x-ray photoemission spectroscopy (HAXPES) technique with an ultracompact built-in Mott-type spin-filter on a sample holder has been developed [5] and employed for the epitaxial CMS thin film, which revealed the high SP (∼90%) at E_F and its almost temperature-independent behavior up to RT, in the bulk region [6]. This result implies that the performances of TMR and GMR would be governed by the electronic and magnetic states near insulator/CMS and metal/CMS interfaces, respectively. In the theoretical investigations based on first-principles calculations on the MgO/CMS interfaces, Sakuma *et al.* [7] reported the decrease of the Co magnetic moment at the interface compared to that in bulk caused by the reduction of the exchange constant near the interface. Miura *et al.* [8] also reported the reduction of the exchange constant in Co near the MgO/CMS interface and a noncollinear magnetic structure near the interface. In the experimental study for the MgO/CMS structure, Tsunegi *et al.* [9] reported that the decrease of the Co magnetic moment in the interface region with respect to that in the inner CMS film by means of the depth-resolved x-ray magnetic circular dichroism (XMCD) in the Co $L_{2,3}$ absorption measurements. Since

*Corresponding author: UEDA.Shigenori@nims.go.jp

†Present address: National Institute for Advanced Industrial Science and Technology, Tsukuba, Ibaraki 305–8568, Japan.

the depth-resolved XMCD in Ref. [9] is obtained from the Co *LMM* Auger electrons with the kinetic energy of $\sim$800 eV, the inelastic mean-free-path (IMFP) of only $\sim$1.4 nm inside CMS estimated from the TPP-2M (Tanuma, Powell, Penn) equation [10] for such electrons seems to be too short to probe both the near-interface and the inner CMS film. In addition, XMCD is useful for detecting the spin and orbital magnetic moments *via* the magneto-optical sum-rule [11,12], but it does not directly give the density of states (DOS) of materials. Therefore, experimental methods, which can detect depth-resolved electronic and magnetic states, are required for the insulator/ferromagnet heterojunctions to clarify the difference in the electronic and magnetic states between the near-interface region and the ferromagnet film inside.

Fecher *et al.* [13] have compared the electronic structures of the CMS(50 nm) films underneath MgO(2 and 20 nm) layers by HAXPES at RT and have demonstrated that the electronic structure around E_F for the CMS film underneath the 20-nm-thick MgO layer is detectable and is almost identical to that underneath the 2-nm-thick MgO layer, which are performed in non-x-ray total reflection (TR) condition to gain a bulk sensitivity. This bulk sensitivity of HAXPES is owing to large IMFP of photoelectrons with the kinetic energy of several keV in solids [14–17]. Thus, an insulator/ferromagnet structure is suitable for exploring its near-interface electronic state around E_F by HAXPES, when IMFP of photoelectrons can be shortened.

There are three possible ways to effectively control IMFP of photoelectrons in solids. The first one is the photon energy-dependent PES measurements. This is because the kinetic energy of the photoelectrons can be tuned by the excitation photon energy and lower kinetic energy of photoelectrons gives shorter IMFP according to the TPP-2M equation. [10] However, the photon energy-dependent valence band PES measurements have a problem in direct comparison of the depth-resolved electronic states, since the photoionization cross-sections of atomic orbitals strongly depend on the photon energy [18–21]. Therefore, direct comparison of the valence band spectra measured with different photon energy needs a careful consideration of the photoionization cross-sections. The second one is the take-off-angle (TOA) dependent HAXPES measurements with a fixed photon energy, since an effective-IMFP (λ) is given by IMFP $\times$ sin(TOA), where TOA is referred to a sample surface. Here, λ corresponds to a depth (d) from surface (or interface), at which the photoelectron intensity given by exp($-d/\lambda$) reduces to $1/e$. In this case, the matrix element effects [22], which depend on experimental geometry and give the angular distribution of photoelectrons for single crystalline samples, affect the valence band spectral shapes in the TOA-dependent measurements [23]. This leads to the difficulty in the direct comparison of the valence band spectra measured with different TOAs. The last one is the use of x-ray TR in HAXPES. The shorter x-ray attenuation length (λ_p) in the TR condition compared to IMFP of several-keV electrons in solids drastically reduces λ in HAXPES at a fixed photon energy as described elsewhere [23]. When the incidence angle (θ) of x-ray with respect to a sample surface in the TR condition is increased by $\sim$1.5°, one can change TR- to non-TR-HAXPES experiments. The small angle change of 1.5°

in HAXPES minimizes the modification of the valence band spectra caused by the matrix element effects, which allows the direct comparison of the valence band spectra for different λ. Therefore, we employed non-TR- and TR-HAXPES to compare buried bulk with near-interface electronic states, respectively, for the insulator/ferromagnet structures. To probe near-interface band dispersion of CMS underneath an AlO$_x$ layer, we employed soft x-ray angle-resolved photoemission spectroscopy (SX-ARPES) in the non-TR condition, because IMFP of photoelectrons detected in SX-ARPES is shorter than λ in TR-HAXPES. In this work, we investigate the electronic and magnetic states of near-interface and buried bulk CMS underneath AlO$_x$ and MgO layers by nondestructive HAXPES in the TR and non-TR conditions. The magnetic states of CMS were measured by magnetic circular dichroism (MCD) in the Co and Mn 2p core-level HAXPES. The magnetizations of Co and Mn in the near-interface region were reduced to $\sim$0.77 times compared to those in the bulk region. The difference in the valence band of CMS between the near-interface and bulk regions was also detected. SX-ARPES for AlO$_x$/CMS film exhibited that even in near interface region, the observed band dispersion was well explained by the bulk band dispersion of CMS.

II. EXPERIMENT

For the HAXPES experiments, two samples of epitaxial CMS films (30 nm) grown on MgO(001) substrates with different capping layers consisting of AlO$_x$(3 nm) and MgO(2 nm) were prepared by DC or RF sputtering at RT. Details of the preparation and characterization of the $L2_1$-ordered CMS films were described elsewhere [6]. On the top of the CMS films, Al(3 nm) and MgO(2 nm) capping layers were deposited individually. The Al and MgO layers were deposited by DC and RF sputtering, respectively. On the top of the MgO layer, an additional Al(1 nm) capping layer was deposited. Then, AlO$_x$ layers were formed by *ex situ* air oxidation in each sample. The coercivity, saturation magnetic moment, and remanent to saturation magnetization (M_R/M_S) ratio of AlO$_x$/CMS/MgO(001) and AlO$_x$/MgO/CMS/MgO(001) structures were deduced to be $\sim$16.5 Oe, $\sim$ 4.3 μ_B, and $\sim$0.97, and $\sim$20.8 Oe, $\sim$ 4.2 μ_B, and $\sim$0.97, respectively, at RT. These values are consistent with those for the epitaxial CMS films reported in the previous work [24]. For the soft x-ray ARPES measurements, an epitaxial CMS film (30 nm) was grown on a Ag(001)/Cr(001)/MgO(001) substrate with the thickness of Ag (Cr) film of 80 (30) nm. Then, an Al(1 nm) capping layer was deposited on the CMS film by DC sputtering. The Al(1 nm) layer was *ex situ* oxidized in air to form an AlO$_x$ layer. The coercivity, saturation magnetization, and M_R/M_S for the CMS film with the Ag/Cr buffer layer at RT were $\sim$10.0 Oe, $\sim$ 4.0 μ_B, and $\sim$0.99, respectively. All the fabricated samples were cut to the in-plane size of 5 mm $\times$ 10 mm with the long side parallel to the [100] direction of the CMS layer.

The HAXPES measurements were conducted at the undulator beamline BL15XU of SPring-8 [17]. The left- or right-handed circularly polarized (LCP or RCP) x-ray (5.95 keV) was used for HAXPES. The degree of LCP and RCP x-rays (P_C) was $\sim$0.95 as described in Ref. [25]. A grazing in-
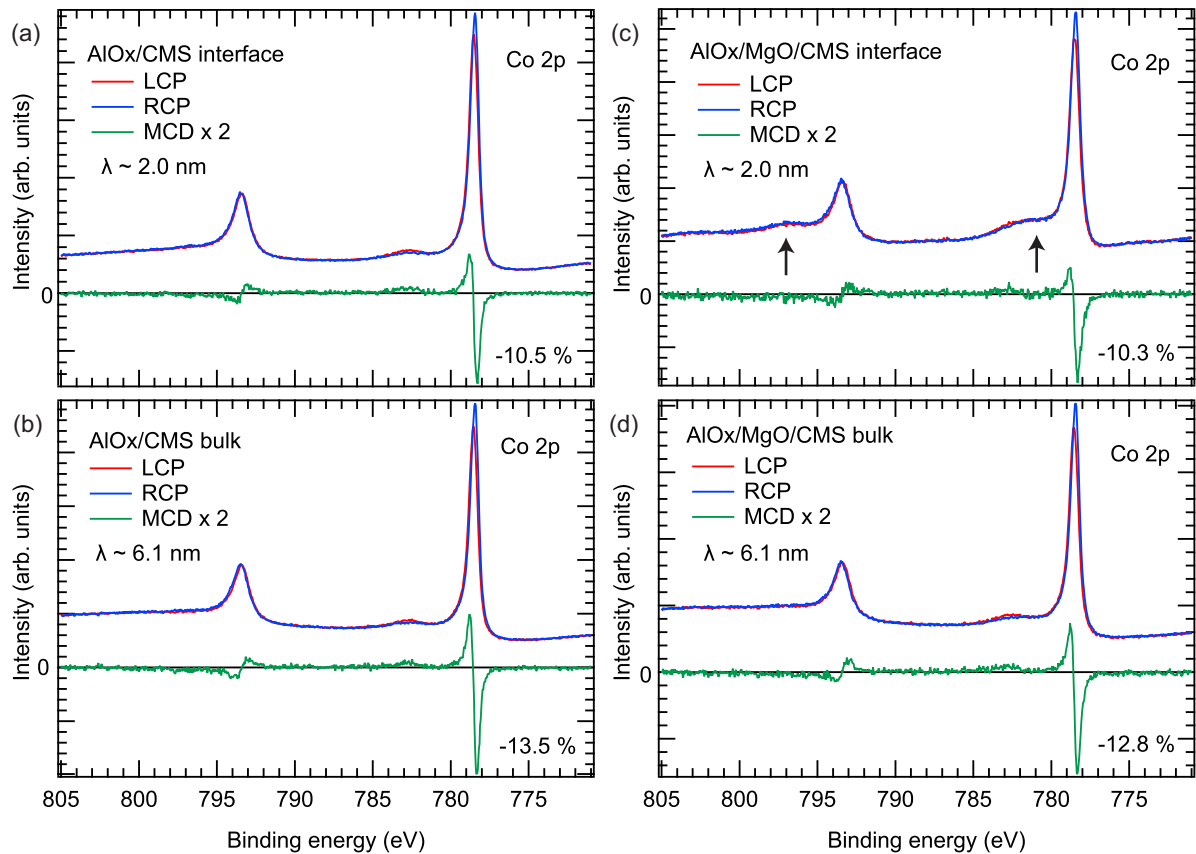
FIG. 1. Co $2p$ core-level MCD-HAXPES spectra of the AlO_x(3 nm) and AlO_x(1 nm)/MgO(2 nm) capped CMS(30 nm)/MgO(001) structures for the non-TR and TR conditions. (a) Near-interface and (b) bulk regions of the CMS film with the AlO_x(3 nm) capping layer. (c) and (d) Same as (a) and (b), respectively, but for the AlO_x(1 nm)/MgO(2 nm) capping layer.

cidence of x-rays with nearly normal emission geometry was employed [17]. Photoelectrons were analyzed and detected by a high-resolution hemispherical electron analyzer (VG Scienta R4000). Total energy resolution was set to 150 meV. The binding energy (E_B) was calibrated by E_F of a Au film. The sample temperature was set to RT (300 K). A magnetic field of 3 kOe was *in situ* applied along the easy magnetization axis ([100] direction of CMS) by a permanent magnet in an analysis chamber, and then the remanent states were probed by HAXPES. The magnetization direction is nearly parallel to the incoming x-rays. The electronic and magnetic states of the near-interface (bulk) region of the CMS thin films were obtained in the TR (non-TR) condition. The incidence angle of x-rays with respect to the sample surfaces was set to 2.0° (0.368°) for the non-TR (TR) condition as referred to the calculated TR critical angle, $\theta_C = 0.505°$, according to Ref. [26]. The footprint of x-rays on the sample was 25 μm × 1.0(5.4) mm in full-width at half-maximum (FWHM) for the non-TR (TR) condition. The IMFPs of photoelectrons in CMS were calculated by the TPP-2M equation [10] and λ was obtained by λ_p IMFP/(λ_p + IMFP), which depended on the incidence angle [23,26].

The SX-ARPES measurements were performed at the twin-helical undulator beamline BL25SU of SPring-8 [27]. Both the LCP and RCP soft x-rays were used simultaneously in SX-ARPES. Therefore, we did not measure the MCD in SX-ARPES. P_C was reported to be ~0.96 [28]. The incidence

angle of soft x-rays was set to 5° with respect to the sample surface. The resultant footprint of x-ray on the sample was approximately 10 μm × 10 μm in FWHM. Photoelectrons were analyzed and detected by a high-resolution hemispherical electron analyzer (VG Scienta DA30). Total energy resolution and angular resolution of SX-ARPES were set to ~80 meV and ~ 0.2°, respectively. The sample temperature was set to 250 K.

III. RESULTS

Figure 1 shows the Co $2p$ core-level HAXPES spectra of the AlO_x and AlO_x/MgO capped CMS thin films obtained using LCP and RCP x-rays. In the TR (non-TR) condition, λ was calculated to be ~2.0 (~6.1) nm in the Co $2p$ core-level region. The intensity difference between the LCP and RCP spectra was defined as MCD. The Co $2p$ HAXPES spectra showed main peaks in the $2p_{3/2}$ and $2p_{1/2}$ regions at E_B of ~778.4 and ~793.5 eV, respectively. A small hump at E_B of ~782.6 eV was found in the spectra and was also commonly seen in the Heusler alloys containing Co atoms [29–32]. The hump structure was slightly larger in the MgO/CMS film for $\lambda \sim 2.0$ nm than the others. Moreover, an additional hump structure was detected in the $2p_{1/2}$ region. These hump structures indicated by the black arrows in Fig. 1(c) were due to oxidation of Co atoms near the MgO/CMS interface. The MCD profiles were similar each other regardless of the cap-
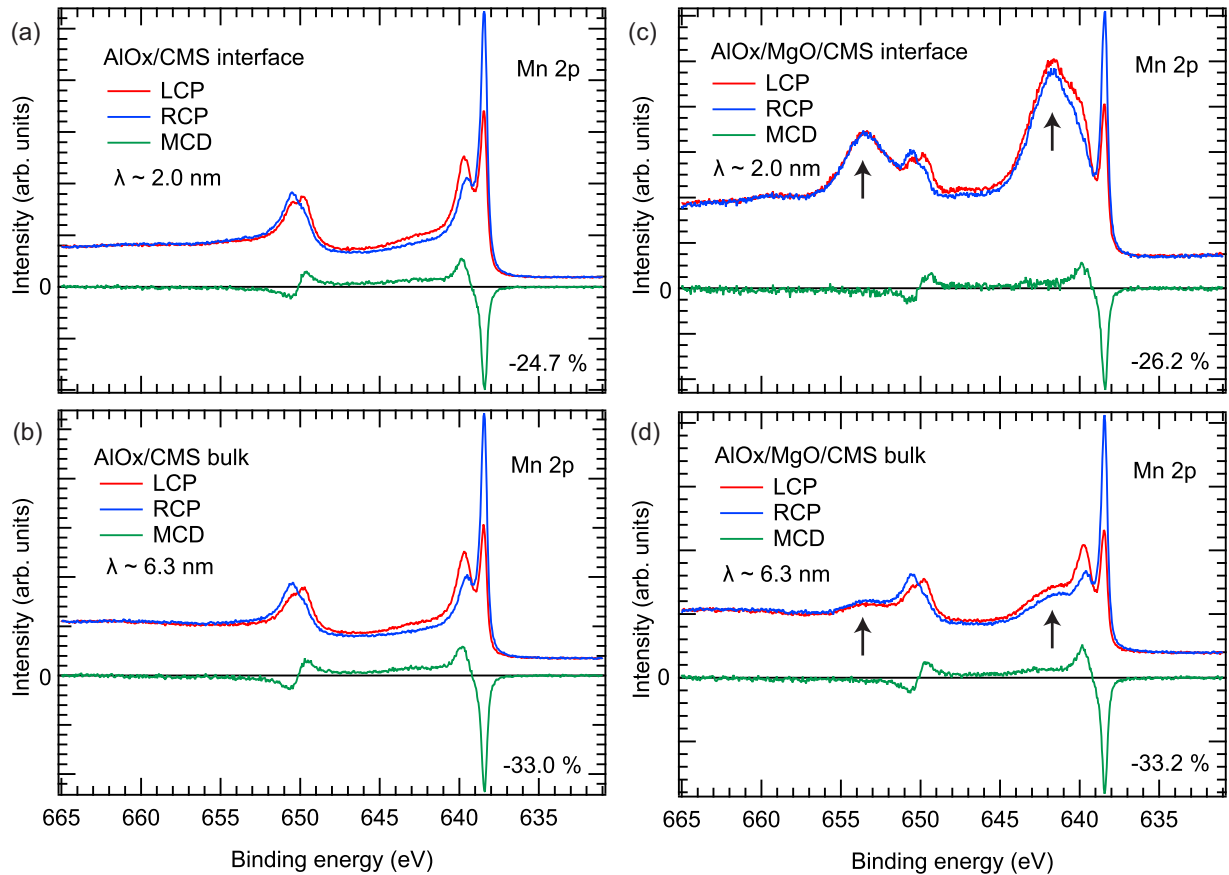
FIG. 2. Mn $2p$ core-level MCD-HAXPES spectra of the AlO_x(3 nm) and AlO_x(1 nm)/MgO(2 nm) capped CMS(30 nm)/MgO(001) structures for the non-TR and TR conditions. (a) Near-interface and (b) bulk regions of the CMS film with the AlO_x(3 nm) capping layer. (c) and (d) Same as (a) and (b), respectively, but for the AlO_x(1 nm)/MgO(2 nm) capping layer.

ping layer or λ, even though oxidation of Co atoms was found in the MgO/CMS interface. A remarkable MCD signal with the negative-to-positive sign change from lower to higher E_B side was found in the Co $2p_{3/2}$ main peak, and the opposite sign change was found in the $2p_{1/2}$ main peak.

Since the magnitude of MCD is proportional to the magnetization projected onto the x-ray propagation direction, we can analyze the element specific magnetization by MCD-HAXPES. When we focused on the negative MCD signal at E_B of $\sim$778.3 eV in the Co $2p_{3/2}$ region in Fig. 1, the MCD given in asymmetry of 13.5–12.8% for $\lambda \sim 6.1$ nm (bulk) reduced to 10.5–10.3% for $\lambda \sim 2.0$ nm (near-interface) in the capped CMS films. Here, the MCD in asymmetry corresponds to the raw MCD divided by the sum of the RCP and LCP spectra after subtracting an integrated-type background. Thus, the magnetization of Co atoms along the [100] direction of CMS near the AlO_x/CMS and MgO/CMS interfaces is reduced to $\sim$0.77 times compared to that of the bulk region of CMS. A similar reduction of the Co magnetization for the MgO/CMS interface was reported in the depth-resolved XMCD in the Co $L_{2,3}$ absorption measurements [9].

Figure 2 shows the Mn $2p$ core-level HAXPES and MCD spectra of the AlO_x and MgO capped CMS films with the calculated λ in the TR (non-TR) condition of $\sim$2.0 ($\sim$6.3) nm. The Mn $2p$ HAXPES spectra of the AlO_x/CMS film for $\lambda \sim 2.0$ and $\sim$6.3 nm were similar each other as shown in

Figs. 2(a) and 2(b). The spectra showed two sharp peaks in the $2p_{3/2}$ region at E_B of $\sim$638.4 and $\sim$639.6 eV and two broad peaks in the $2p_{1/2}$ region at E_B of $\sim$649.8 and $\sim$650.4 eV. For the MgO/CMS film, the Mn $2p$ spectra showed additional broad peaks indicated by the black arrows in Figs. 2(c) and 2(d). Moreover, the intensity of the broad peaks strongly enhanced in the spectrum for $\lambda \sim 2.0$ nm compared to that for $\lambda \sim 6.3$ nm. These broad peaks attribute to oxidation of Mn atoms near the MgO/CMS interface. This result suggests that the Mn atoms near the MgO/CMS interface are strongly oxidized, which would be induced by a degraded interface of MgO/CMS prepared by a sputtering deposition of MgO on CMS [33]. By assuming an exponential decay of the photoemission intensity as a function of depth and the oxidized Mn atoms concentrated below the MgO layer, the thickness of oxidized CMS film is estimated to be $\sim$1.5 nm. Note that the Si $2s$ core-level HAXPES spectra for the MgO/CMS film also showed significant oxidation near the interface (not shown).

As can be seen in Fig. 2, the MCD profiles for the AlO_x/CMS and MgO/CMS films were similar each other regardless of oxidation or λ. A remarkable MCD signal with the negative-to-positive sign change from lower to higher E_B side was found in the Mn $2p_{3/2}$ region, and the opposite sign change was found in the $2p_{1/2}$ region. Since the components of oxidized Mn atoms in the Mn $2p$ HAXPES spectra did not show an additional MCD feature, the oxidized Mn atoms
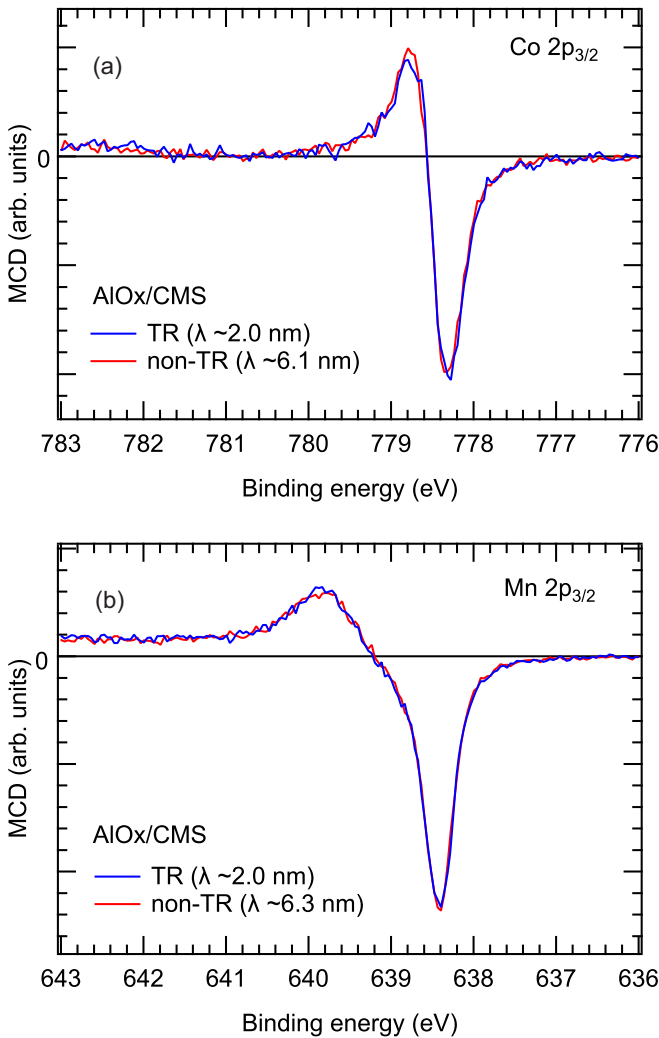
FIG. 3. Enlarged MCD spectra of (a) the Co $2p_{3/2}$ and (b) Mn $2p_{3/2}$ regions for the AlO$_x$(3 nm)/CMS(30 nm)/MgO(001) structure. The spectra measured in the TR (non-TR) condition are indicated by blue (red) lines. In both (a) and (b), the spectra were normalized at the negative MCD signals for comparison.

FIG. 4. Valence band HAXPES spectra of the AlO$_x$(3 nm) and AlO$_x$(1 nm)/MgO(2 nm) capped CMS(30 nm)/MgO(001) structures for the non-TR and TR conditions. The dotted curves are identical to the valence band spectrum of bulk region of CMS with the AlO$_x$(3 nm) capping layer and are superimposed on the other spectra for comparison.

would be in a paramagnetic or antiferromagnetic state, that is, the magnetization of the oxidized Mn atoms along the [100] direction was vanished. The Mn $2p$ MCD at E_B of $\sim$638.4 eV of 33.0–33.2% for $\lambda \sim 6.3$ nm (bulk) reduced to 24.7–26.2% for $\lambda \sim 2.0$ nm (near-interface). Here, the MCD signal in the AlO$_x$/MgO/CMS structure came from the CMS film underneath the oxidized CMS layer. Thus, the magnetization of Mn atoms along the [100] direction near the AlO$_x$/CMS and oxidized CMS/CMS interfaces was reduced to $\sim$0.76 times compared to that of CMS in the bulk region. This reduction factor was comparable to the case of the Co atoms.

Figure 3 compares the MCD profiles in the Co $2p_{3/2}$ and Mn $2p_{3/2}$ core levels for the near-interface and bulk regions of the AlO$_x$/CMS film. Here, the comparison of MCD profiles for the MgO/CMS film is ignored, since the oxidized CMS layer exists between the MgO and CMS layers. The MCD profiles are normalized at the huge negative MCD in each region. One sees that the MCD profiles for the near-interface and bulk regions are identical each other in both the Co and
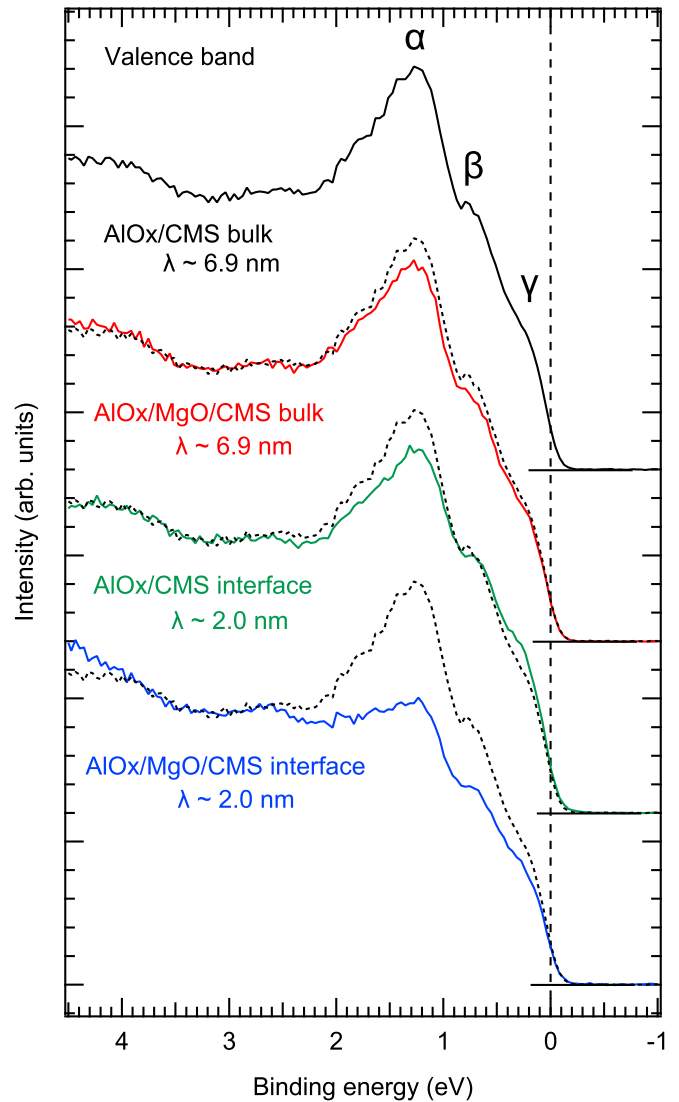
Mn $2p_{3/2}$ regions within the statistical errors in the MCD intensity. The energy splitting between the negative and positive MCD signals is caused by the spin exchange interaction between the $2p$ core-hole and $3d$ electrons in the photoemission final states and is proportional to the magnitude of magnetic moment [34], that is, a larger local magnetic moment leads to a larger energy splitting in MCD-HAXPES [35]. Therefore, the magnetizations of Co and Mn along the [110] direction was reduced in near-interface region, although the magnitudes of magnetic moments of Co and Mn in near-interface region are comparable to those in the bulk region, respectively, for the AlO$_x$/CMS film.

Figure 4 shows the valence band spectra of the AlO$_x$/CMS and MgO/CMS films with the calculated λ of $\sim$2.0 and $\sim$6.9 nm. Each spectrum was obtained by the sum of LCP and RCP spectra after subtracting an integrated-type background.
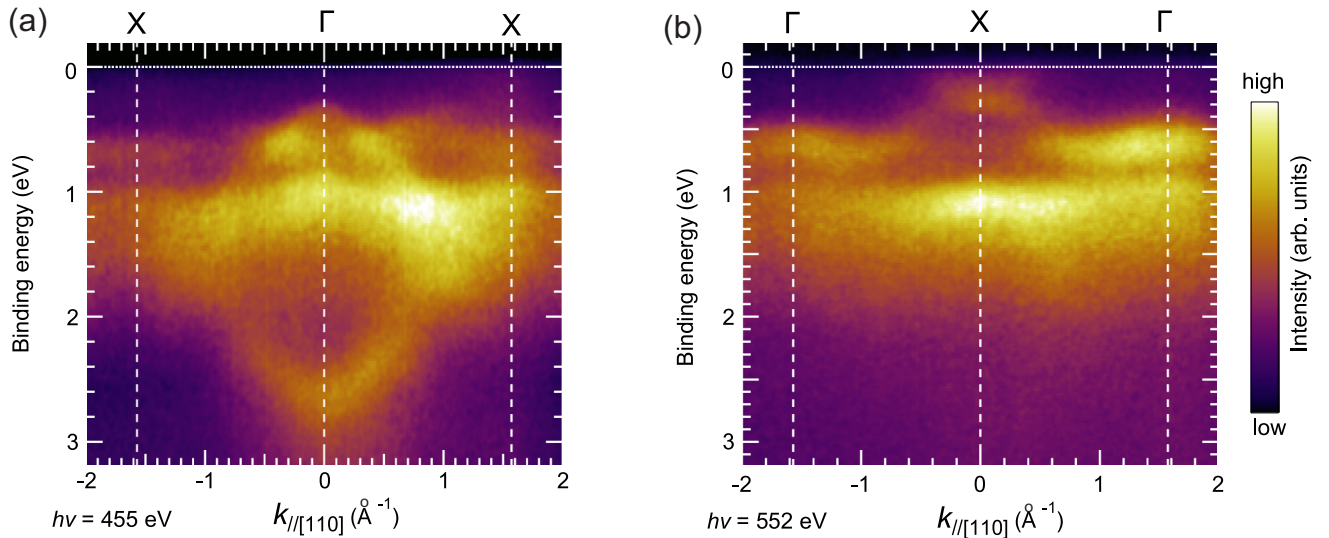
FIG. 5. SX-ARPES intensity maps along the Γ-K-X direction for the AlO$_x$(1 nm) capped CMS(001) film with the excitation photon energy ($h\nu$) of (a) 455 and (b) 552 eV at 250 K with IMFP of $\sim$1.0 nm. The horizontal dotted lines indicate E_F. The vertical dashed lines indicate the high symmetry points (Γ or X).

The spectra were normalized at the hump structure located at E_B of 2.6 eV, for comparison. The spectra consisted of three structures below 2 eV; the main peak (labeled by α) and two shoulders (labeled by β and γ). These structures were also found in the previous HAXPES spectra for CMS [13]. The valence band spectra for the AlO$_x$/CMS and MgO/CMS films in the bulk region ($\lambda \sim 6.9$ nm) were similar each other, while the peak α and shoulder β slightly reduced in the MgO/CMS film. The slight reduction in the MgO/CMS film was mainly caused by the presence of Mn-oxides, which reduced the metallic Mn DOS near the interface. In fact, the valence band spectrum of the MgO/CMS film near the interface ($\lambda \sim 2.0$ nm) showed a significant reduction of α and β and a slight reduction of γ by the increase of the Mn oxides as seen in the Mn $2p$ spectra in Fig. 2(c). For the near-interface valence band spectrum of the AlO$_x$/CMS film ($\lambda \sim 2.0$ nm), a slight decrease (increase) of α (γ) compared to the spectrum for the AlO$_x$/CMS film ($\lambda \sim 6.9$ nm) was found, while Co and Mn oxides were obviously invisible in the Co and Mn $2p$ spectra in Figs. 1(a) and 2(a). This result indicates that in the AlO$_x$/CMS film, the near-interface electronic structure is different from the bulk one as well as the difference in the magnetization between the near-interface and bulk regions. Furthermore, the effects of defects or off-stoichiometry to the electronic structure near the interface in the AlO$_x$/CMS film is negligibly weak, if any. It is obvious that the energy shift of α, β, and γ structures is very small. If defects or off-stoichiometry exists near the interface, the total electron number in the unit cell changes and the chemical potential shift (the energy shift of α, β and γ structures) occurs.

Figure 5 shows the SX-ARPES results for the AlO$_x$(1 nm)/CMS(001) sample with the excitation photon energies of 455 and 552 eV measured at 250 K. At these photon energies, IMFP was calculated to be $\sim$1.0 nm. This value is half of λ in TR-HAXPES. The normal emission from the (001) surface corresponds to the Γ-X direction in the reciprocal space. One

sees a clear photon energy dependence in the ARPES results in the figures. In Fig. 5(a), the observed band dispersion measured at the excitation energy of 455 eV is symmetrical to $k_{//[110]}$ and a convex band dispersion with the apex located at 0.24 eV and Γ point originated from the minority spin states, which are expected from the band dispersion calculations for bulk CMS [36–38]. The energy of 0.24 eV is very close to the minority spin valence band maximum reported in spin-resolved HAXPES for CMS at 300 K [6]. In addition, the weak intensity across E_F is seen at the X point due to the majority spin states. In contrast to Fig. 5(a), the band dispersion measurement at the excitation energy of 552 eV in Fig. 5(b) exhibits a clear "X"-shaped band dispersion at the X point near E_F and the weakened intensity at the apex of the convex band dispersion due to the minority spin states. These band features are very similar to the results in SX-ARPES for bulk Co$_2$MnGe [39] as a predicted half-metal [36]. A clear photon-energy-dependent band dispersion suggests that three-dimensional bulk band structure is remained in the near-interface region (IMFP$\sim$1.0 nm) for the AlO$_x$/CMS sample. Note that we cannot find surface resonances located near E_F at around the Γ point, which has been reported in SX-ARPES for an AlO$_x$/CMS structure by Lidig *et al.* [40].

IV. DISCUSSION

Since the MgO/CMS interface consists of the oxidized CMS layer underneath MgO layer in contrast to the AlO$_x$/CMS interface, in the following, we discuss the near-interface electronic and magnetic states of the AlO$_x$/CMS film. When the single magnetic domain structure near the interface of the AlO$_x$/CMS film is assumed owing to the high M_R/M_S ratio of 0.97, we consider a possible mechanism of the reduction of the magnetization near the interface according to the theoretical work on the surface magnetism [41]. For bare ferromagnetic films, it is expected that an exchange interaction at a surface (J_S) differs from that in a bulk region (J_B),

since the environment of the magnetic moments at the surface differs from that in the bulk region. According to Ref. [41], in the case of that $J_S/J_B = 0.1$ on the path perpendicular to the surface and $J_S/J_B = 1.0$ on the path parallel to the surface at the temperature of $0.3T_C$, the magnetization at the surface reduces to 0.8 times compared to the bulk magnetization owing to thermal spin-wave excitations near the surface. When the interactions at the interface between the AlO$_x$ and CMS films to the magnetic properties are negligible, the temperature of $0.3T_C$ and the reduction of magnetization (0.8) in the calculation [41] are very close to RT/T_C of 0.304 for the CMS films and the observed reduction (~ 0.77) in the Co and Mn MCD signals near the interface in our experiments, respectively. Therefore, the reduced magnetization near the interface of AlO$_x$/CMS film is due to possible enhanced spin-wave excitations. The enhanced spin-wave excitations near the interface of the CMS film is virtually comparable to the increase of temperature in the bulk region to satisfy Bloch's $T^{3/2}$ law in terms of spin-wave excitations. It is expected that the fraction of the Co e_g and t_{2g} partial DOSs can change [6], when the temperature of CMS increases. This fraction change can reduce the peak α in the valence band spectrum of CMS in Fig. 4 for the CMS film near the interface compared to that in the bulk region.

The spin-wave excitations (or precessions) of local magnetic moments only change the magnetizations along the easy magnetization axis. That is, the magnitude of local magnetic moment is unchanged by the spin-wave excitations. As seen in Fig. 3, the magnitude of Co (Mn) local magnetic moment is almost identical for the near-interface and bulk regions in the AlO$_x$/CMS structure. Nawa *et al.* [42] reported the temperature-dependent spin-dependent DOS for bulk CMS by means of the density functional theory calculations with the disordered local moment method, which treats the fluctuation of local magnetic moments at finite temperature. In other words, they treated the fluctuation as a substitution of the precession (or spin-wave excitation) of the local magnetic moments. As seen in Fig. 3 in Ref. [42] for $L2_1$-ordered CMS, the majority spin DOS peak at 1 eV corresponding to the peak α in Fig. 4 decreases with increasing temperature. In addition, the majority spin DOS subpeak at 0.5 eV in Ref. [42] corresponding to shoulder structure β in Fig. 4 slightly shifts toward to E_F with increasing temperature. In the minority spin DOS near E_F, the DOS gradually increases with increasing temperature, while changes of the majority spin DOS near E_F are insensitive to temperature. This causes the increase of DOS near E_F with increasing temperature. These tendencies are consistent with the difference in the valence band spectra between the near-interface and bulk region for AlO$_x$/CMS structure. That is, in the AlO$_x$/CMS structure, the reduced intensity of peak α, slight shift of shoulder structure β, and slight increase of shoulder structure γ for the near-interface valence band spectrum compared to the valence band spectrum for the bulk region as shown in Fig. 4. Therefore, it is a plausible origin for the spin-wave excitations that are enhanced due to the weakened exchange interaction between the local magnetic moments near the interface region of the AlO$_x$/CMS structure, which leads the difference in the electronic and magnetic states between the near-interface and bulk regions.

In the above-discussion, we did not consider an interface-induced magnetic anisotropy (IMA) at an insulator/ferromagnet interface as is similar to a surface-induced magnetic anisotropy in a ferromagnetic thin film [41]. The IMA can cause that the magnetization inclines toward to the direction perpendicular to the film plane near the interface, even if the in-plane easy magnetization axis of the film is realized (in other words, noncollinear magnetization) [34,43]. In addition, at the insulator/ferromagnetic interfaces, where AlO$_x$ or MgO is used as an insulator, the perpendicular magnetization is introduced by a strong IMA, when the ferromagnetic film thickness is less than 1 nm [44–47]. In our experiments, the inclined magnetization near the interface is also expected, if the reduced net magnetization near the interface is due to the noncollinear magnetization caused by the IMA, since the CMS film is sufficiently thicker than 1 nm. As mentioned above, the magnitude of MCD is proportional to the magnetization projected onto the propagation direction of x-rays, the inclined magnetization can reduce the MCD signal near the interface. Therefore, the PMA can be another possible mechanism in the reduction of magnetization near the interface in the AlO$_x$/CMS structure.

When the noncollinear magnetization near interface due to strong PMA induced by the IMA is realized, not the magnetization but the magnitude of local magnetic moment is expected to be slightly enhanced as reported in the perpendicularly magnetized MgO/Fe [34,48] and MgO/CMS films [49]. In both cases, ultrathin Fe and CMS magnetic films underneath the MgO layer are used, and the increase of the local magnetic moment induced by the interfacial effects is found. In contrast, as can be seen in Fig. 3, the magnitude of Co (Mn) local magnetic moment near-interface and bulk regions is almost identical each other in the AlO$_x$/CMS structure. Therefore, we may conclude that the reduction of the magnetizations of Co and Mn near the interface is not due to the IMA.

Finally, we consider the highly spin-polarized surface resonances in the bare and AlO$_x$-capped CMS(001) reported in Refs. [4] and [40], respectively. Jourdan *et al.* [4] have reported the high SP of $\sim 93\%$ at E_F for the bare CMS(001) film by means of surface-sensitive spin-resolved PES at RT with the excitation energy of 21.2 eV. This high SP is inconsistent with the reduction of the magnetization (~ 0.77) near interface of the AlO$_x$/CMS structure in this work, when we assume that SP of 100% in the bulk region is realized at RT and that SP is proportional to the magnetization. In this assumption, the expected SP near the interface is $\sim 77\%$. In contrast, the similar SP for bare CMS(001) has been found in surface-sensitive spin-resolved PES using the *s*-polarized light with the energy of 37 eV at RT [50]. In Ref. [50], spin-resolved PES with the photon energy dependence (30–70 eV) has also been performed, and the signature of surface resonance in CMS is not clearly observed. The discrepancy between Refs. [4] and [50] might be caused by the difference in the probed momentum space, because $k_{//[001]}$ depends on the excitation photon energy, in principle. At the excitation energy of 21.2 eV, $k_{//[001]}$ is out of the Γ point, which misleads to high SP as described in Ref. [50].

Although the SX-ARPES results on the AlO$_x$/CMS film reported in Ref. [40] show the surface resonance near E_F, the

SX-ARPES results in this work (Fig. 5) showed no obvious surface resonance. We are aware of that the results agree well with the corresponding band dispersion for Co_2MnGe (Fig. 4 in Ref. [39]) and also with the dispersion for Co_2MnSi reported in Ref. [40], but only if the assignment of the Γ and X points is reversed, such that the Γ point in $k_{//[001]}$ at an integer multiple of the reciprocal lattice vector length confused the identification of the Γ and X points. When the assigned X point is corrected to the Γ point in the bottom panel of Fig. 3 in Ref. [40], the observed band dispersion is very similar to our SX-ARPES result shown in Fig. 5(b), that is, a metallic band dispersion at the X point and no band dispersion near E_F at the Γ point. The confusion of the Γ and X points in Ref. [40] is also confirmed by the $k_{//[001]}$-dependent SX-ARPES result for bulk Co_2MnGe [39], which has the $L2_1$ structure with a similar lattice parameter and half-metallicity. Therefore, we can conclude that the surface resonance is not an origin of the difference of the electronic and magnetic states between the near-interface and bulk regions of the AlO_x/CMS structure.

In Fig. 4, the shoulder structure γ in the valence band spectrum for the near-interface region of the AlO_x/CMS structure is slightly larger than that for the bulk region, but the SX-ARPES results shown in Fig. 5 do not show any additional band states near E_F due to the slight increase of γ. If the origin of slight increase of γ arises from the enhanced spin-wave excitations (or enhanced fluctuation of local magnetic moments), s-orbital-like minority spin states around E_F are introduced by the fluctuation of local magnetic moments according to Ref. [8]. Since the photoionization cross-section ratio of the s orbital to d orbital in the valence region for the $3d$ transition metal is very large in HAXPES [25] but small in SX-PES [21], the higher sensitivity to the s orbital in HAXPES can detect the s orbital states induced by the fluctuation, even if the states are quite small. In contrast, the lower sensitivity to the s orbital in SX-PES cannot detect the quite small s orbital states. Or there is a possibility that such s states are missing in the SX-ARPES results in Fig. 5 due to that the probed momentum space is limited in the Γ-X direction, whereas HAXPES gives the Brillouin zone averaged spectra.

From the above discussion, we can conclude that the reasonable origin of the differences in the electronic and magnetic states between the near-interface and bulk region of the AlO_x/CMS structure is the enhanced spin-wave excitations near the interface compared to the bulk region. When the TMR ratios in many TMR junctions [1] are governed by the magnetization near the interface, the strong reduction of TMR ratio with increasing temperature can be understood by a faster reduction of the magnetization along the easy magnetization

direction near the interface with increasing temperature originated from the enhanced spin-wave excitations as compared to the bulk magnetization.

V. SUMMARY

In summary, we conducted the depth-dependent HAXPES measurements for the AlO_x/CMS and AlO_x/MgO/CMS structures to clarify the differences in the electronic and magnetic states between the near-interface and bulk regions for the CMS films utilizing the TR and non-TR conditions. TR-HAXPES combined with MCD can clearly detect the near-interface electronic and magnetic states of the CMS films. At the MgO/CMS interface, a strong oxidation of the Mn and Si atoms underneath the MgO layer and no oxidation underneath the AlO_x layer were experimentally detected by nondestructive HAXPES combined with TR. The Co and Mn $2p$ core-level MCD-HAXPES measurements for the near-interface and bulk regions of the AlO_x/CMS film clearly revealed that the Co and Mn magnetizations along the [100] direction near the interface reduce to ∼0.77 times with respect to those in the bulk region. We can conclude that the possible origin of the reduction of the Co and Mn magnetizations and the changes in the valence band profile near the AlO_x/CMS interface compared to the CMS film in the bulk region is the enhanced spin-wave excitations due to the weakened exchange interaction, which can slightly modify the valence band electronic states, near the interface, by considering precession of local magnetic moments at a finite temperature. Thus, the combination of HAXPES with TR is very useful for exploring the electronic and magnetic states of near-interface and bulk regions for the insulator/ferromagnet heterojunctions in the nondestructive way.

[1] K. Elphick, W. Frost, M. Samiepour, T. Kubota, K. Takanashi, H. Sukegawa, S. Mitani, and A. Hirosawa, Heusler alloys for spintronic devices: Review on recent development and future perspectives, Sci. Technol. Adv. Mater. **22**, 235 (2021).

[2] B. Hu, K. Moges, Y. Honda, H.-x. Liu, T. Uemura, M. Yamamoto, J.-i. Inoue, and M. Shirai, Temperature dependence of spin-dependent tunneling conductance of magnetic tunnel

junctions with half-metallic Co_2MnSi electrodes, Phys. Rev. B **94**, 094428 (2016).

[3] J. W. Jung, Y. Sakuraba, T. Sasaki, Y. Miura, and H. Hono, Enhancement of magnetoresistance by inserting thin NiAl layers at the interfaces in $Co_2FeGa_{0.5}Ge_{0.5}$/Ag/$Co_2FeGa_{0.5}Ge_{0.5}$ current-perpendicular-to-plane pseudo spin valves, Appl. Phys. Lett. **108**, 102408 (2016).

[4] M. Jourdan J. Minar, J. Braun, A. Kronenberg, S. Chadov, B. Balke, A. Gloskovskii, M. Kolbe, H. J. Elmers, G. Schönhense, H. Ebert, C. Felser, and M. Klaui, Direct observation of half-metallicity in the Heusler compound Co$_2$MnSi, Nat. Commun. **5**, 3974 (2014).

[5] S. Ueda and Y. Sakuraba, Direct observation of spin-resolved valence band electronic states from a buried ferromagnetic layer with hard x-ray photoemission, Sci. Technol. Adv. Mater. **22**, 317 (2021).

[6] S. Ueda, Y. Miura, Y. Fujita, and Y. Sakuraba, Direct probing of temperature-independent bulk-halfmetallicity in Co$_2$MnSi by spin-resolved hard x-ray photoemission, Phys. Rev. B **106**, 075101 (2022).

[7] A. Sakuma, Y. Toga, and H. Tsuchiura, Theoretical study on the stability of magnetic structures in the surface and interfaces of Heusler alloys, Co$_2$MnAl and Co$_2$MnSi, J. Appl. Phys. **105**, 07C910 (2009).

[8] Y. Miura, K. Abe, and M. Shirai, Effects of interfacial non-collinear magnetic structures on spin-dependent conductance in Co$_2$MnSi/MgO/Co$_2$MnSi magnetic tunnel junctions: A first-principles study, Phys. Rev. B **83**, 214411 (2011).

[9] S. Tsunegi, Y. Sakuraba, K. Amemiya, M. Sakamaki, E. Ozawa, A. Sakuma, K. Takanashi, and Y. Ando, Observation of magnetic moments at the interface region in magnetic tunnel junctions using depth-resolved x-ray magnetic circular dichroism, Phys. Rev. B **85**, 180408(R) (2012).

[10] S. Tanuma, C. J. Powell, and D. R. Penn, Calculations of electron inelastic mean free paths. V. Data for 14 organic compounds over the 50–2000 eV range, Surf. Interf. Anal. **21**, 165 (1994).

[11] B. T. Thole, P. Carra, F. Sette, and G. van der Laan, x-ray circular dichroism as a probe of orbital magnetization, Phys. Rev. Lett. **68**, 1943 (1992).

[12] P. Carra, B. T. Thole, M. Altarelli, and X. Wang, X-ray circular dichroism and local magnetic fields, Phys. Rev. Lett. **70**, 694 (1993).

[13] G. H. Fecher, B. Balke, A. Gloskowskii, S. Ouardi, C. Felser, T. Ishikawa, M. Yamamoto, Y. Yamashita, H. Yoshikawa, S. Ueda, and K. Kobayashi, Detection of the valence band in buried Co$_2$MnSi-MgO tunnel junctions by means of photoemission spectroscopy, Appl. Phys. Lett. **92**, 193513 (2008).

[14] Y. Takata, M. Yabashi, K. Tamasaku, Y. Nishino, D. Miwa, T. Ishikawa, E. Ikenaga, K. Horiba, S. Shin, M. Arita, K. Shimada, H. Namatame, M. Taniguchi, H. Nohira, T. Hattori, S. Sodergren, B. Wannberg, and K. Kobayashi, Development of hard x-ray photoelectron spectroscopy at BL29XU in SPring-8, Nucl. Instrum. Methods Phys. Res. Sect. A. **547**, 50 (2005).

[15] K. Kobayashi, M. Yabashi, Y. Takata, T. Tokushima, S. Shin, K. Tamasaku, D. Miwa, T. Ishikawa, H. Nohira, T. Hattori, Y. Sugita, O. Nakatsuka, S. Sakai, and S. Zaima, High resolution-high energy x-ray photoelectron spectroscopy using third-generation synchrotron radiation source, and its application to Si-high k insulator systems, Appl. Phys. Lett. **83**, 1005 (2003).

[16] C. S. Fadley, Hard x-ray photoemission with angular resolution and standing-wave excitation, J. Electron Spectrosc. Rel. Phenom. **190**, 165 (2013).

[17] S. Ueda, Application of hard x-ray photoelectron spectroscopy to electronic structure measurements for various functional materials, J. Electron Spectrosc. Rel. Phenom. **190**, 235 (2013).

[18] J. H. Scofield, Theoretical photoionization cross sections from 1 to 1500 keV, Tech. Rep. UCRL-51326 (Lawrence Livermore Laboratory, 1973).

[19] M. B. Trzhaskovskaya, V. I. Nefedov, and V. G. Yarzhemsky, Photoelectron angular distribution parameters for elements $Z = 1$ to $Z = 54$ in the photoelectron energy range 100–5000 eV, At. Data Nucl Data Tables **77**, 97 (2001).

[20] M. B. Trzhaskovskaya, V. K. Nikulin, V. I. Nefedov, and V. G. Yarzhemsky, Non-dipole second order parameters of the photoelectron angular distribution for elements $Z = 1-100$ in the photoelectron energy range 1–10 keV, At. Data Nucl. Data Tables **92**, 245 (2006).

[21] J. J. Yeh and I. Lindau, Atomic subshell photoionization cross sections and asymmetry parameters: $1 \leqslant Z \leqslant 103$, At. Data Nucl, Data Tables **32**, 1 (1985).

[22] S. M. Goldberg, C. S. Fadley, and S. Kono, Photoionization cross-sections for atomic orbitals with random and fixed spatial orientation, J. Electron Spectrosc. Rel. Phenom. **21**, 285 (1981).

[23] S. Ueda, Depth-resolved electronic structure measurements by hard x-ray photoemission combined with x-ray total reflection: Direct probing of surface band bending of polar GaN, Appl. Phys. Express **11**, 105701 (2018).

[24] H. Kijima, T. Ishikawa, T. Marukame, H. Koyama, K.-i. Matsuda, T. Uemura, and M. Yamamoto, Epitaxial growth of full-Heusler alloy Co$_2$MnSi thin films on MgO-buffered MgO substrates, IEEE Trans. Magn. **42**, 2688 (2006).

[25] S. Ueda and I. Hamada, Polarization dependent bulk-sensitive valence band photoemission spectroscopy and density functional theory calculations: Part I. 3d transition metals, J. Phys. Soc. Jpn. **86**, 124706 (2017).

[26] B. L. Henke, E. M. Gullikson, and J. C. Davis, X-ray interactions: Photoabsorption, scattering, transmission, and reflection at $E = 50–30,000$ eV, $Z = 1–92$, At. Data Nucl. Data Tables **54**, 181 (1993).

[27] T. Muro, Y. Senba, H. Ohashi, T. Ohkochi, T. Matsushita, T. Kinoshita, and S. Shin, Soft x-ray ARPES for three-dimensional crystals in the micrometre region, J. Synchrotron Rad. **28**, 1631 (2021).

[28] T. Hirono, H. Kimura, T. Muro, Y. Saitoh, and T. Ishikawa, Full polarization measurement of SR emitted from twin helical undulators with use of Sc/Cr multilayers at near 400 eV, J. Electron Spectrosc. Rel. Phenom. **144** 1097 (2005).

[29] J. Barth, G. H. Fecher, B. Balke, S. Ouardi, T. Graf, C. Felser, A. Shkabko, A. Weidenkaff, P. Klaer, H. J. Elmers, H. Yoshikawa, S. Ueda, and K. Kobayashi, Itinerant half-metallic ferromagnets Co$_2$TiZ ($Z =$ Si, Ge, Sn): *Ab initio* calculations and measurement of the electronic structure and transport properties, Phys. Rev. B **81**, 064404 (2010).

[30] S. Ouardi, G. H. Fecher, B. Balke, A. Beleanu, X. Kozina, G. Stryganyuk, C. Felser, W. Klöß, H. Schrader, F. Bernardi, J. Morais, E. Ikenaga, Y. Yamashita, S. Ueda, and K. Kobayashi, Electronic and crystallographic structure, hard x-ray photoemission, and mechanical and transport properties of the half-metallic Heusler compound Co$_2$MnGe, Phys. Rev. B **84**, 155122 (2011).

[31] J. Winterlik, G. H. Fecher, B. Balke, T. Graf, V. Alijani, V. Ksenofontov, C. A. Jenkins, O. Meshcheriakova, C. Felser, G. Liu, S. Ueda, K. Kobayashi, T. Nakamura, and M. Wójcik, Electronic, magnetic, and structural properties of the ferrimagnet Mn$_2$CoSn, Phys. Rev. B **83**, 174448 (2011).

[32] R. Fetzer, S. Ouardi, Y. Honda, H.-x. Liu, S. Chadov, B. Balke, S. Ueda, M. Suzuki, T. Uemura, M. Yamamoto, M. Aeschlimann, M. Cinchetti, G. H. Fecher, and C. Felser, Spin-resolved low-energy and hard x-ray photoelectron spectroscopy of off-stoichiometric Co$_2$MnSi Heusler thin films exhibiting a record TMR, J. Phys. D **48**, 164002 (2015).

[33] S. Tsunegi, Y. Sakuraba, M. Oogane, N. D. Telling, L. R. Shelford, E. Arenholz, G. van der Laan, R. J. Hicken, K. Takanashi, and Y. Ando, Tunnel magnetoresistance in epitaxially grown magnetic tunnel junctions using Heusler alloy electrode and MgO barrier, J. Phys. D **42**, 195004 (2009).

[34] S. Ueda, M. Mizuguchi, M. Tsujikawa, and M. Shirai, Electronic structures of MgO/Fe interfaces with perpendicular magnetization revealed by hard x-ray photoemission with an applied magnetic field, Sci. Technol. Adv. Mater. **20**, 796 (2019).

[35] X. Kozina, G. H. Fecher, G. Stryganyuk, S. Ouardi, B. Balke, C. Felser, G. Schönhense, E. Ikenaga, T. Sugiyama, N. Kawamura, M. Suzuki, T. Taira, T. Uemura, M. Yamamoto, H. Sukegawa, W. Wang, K. Inomata, and K. Kobayashi, Magnetic dichroism in angle-resolved hard x-ray photoemission from buried layer, Phys. Rev. B **84**, 054449 (2011).

[36] S. Picozzi, A. Continenza, and A. J. Freeman, Co$_2$MnX ($X =$ Si, Ge, Sn) Heusler compounds: An *ab initio* study of their structural, electronic, and magnetic properties at zero and elevated pressure, Phys. Rev. B **66**, 094421 (2002).

[37] G. Qion, W. Ren, and D. J. Singh, Interplay of local moment and itinerant magnetism in cobalt-based Heusler ferromagnets: Co$_2$TiSi, Co$_2$MnSi, and Co$_2$FeSi, Phys. Rev. B **101**, 014427 (2020).

[38] S. Chernov, C. Lidig, O. Fedchenko, K. Medjianik, S. Babenkov, D. Vasilyev, M. Jourdan, G. Schönhense, and H. J. Elmers, Band structure tuning of Heusler compounds: Spin- and momentum-resolved electronic structure analysis of compounds with different band filling, Phys. Rev. B **103**, 054407 (2021).

[39] T. Kono, M. Kakoki, T. Yoshikawa, X. Wang, K. Goto, T. Muro, R. Umetsu, and A. Kimura, Visualizing half-metallic bulk band structure with multiple Weyl cones of the Heusler ferromagnet, Phys. Rev. Lett. **125**, 216403 (2020).

[40] C. Lidig, J. Minár, J. Braun, H. Ebert, A. Gloskovskii, J. A. Krieger, V. Strocov, M. Kläui, and M. Jourdan, Surface resonance of thin films of the Heusler half-metal Co$_2$MnSi probed

by soft x-ray angular resolved photoemission spectroscopy, Phys. Rev. B **99**, 174432 (2019).

[41] H. C. Siegmann, Surface and 2D magnetism, J. Phys.: Condens. Mater. **4**, 8395 (1992).

[42] K. Nawa, I. Kurniawan, K. Masuda, Y. Miura, C. E. Patrick, and J. B. Staunton, Temperature-dependent spin polarization of Heusler Co$_2$MnSi from the disordered local-moment approach: Effects of atomic disorder and nonstoichiometry, Phys. Rev. B **102**, 054424 (2020).

[43] T. Kawauchi, Y. Miura, X. Zhang, and K. Fukutani, Interface-driven noncolliner magnetic structure and phase transition of Fe thin films, Phys. Rev. B **95**, 014432 (2017).

[44] S. Monso, B. Rodmacq, S. Aiffret, G. Casali, F. Fettar, B. Gilles, B. Dieny, and P. Boyer, Crossover from in-plane to perpendicular anisotropy in Pt/CoFe/AlO$_x$ sandwiches as a function of Al oxidation: A very accurate control of the oxidation of tunnel barriers, Appl. Phys. Lett. **80**, 4157 (2002).

[45] B. Rodmacq, A. Manchon, C. Ducruet, S. Aiffret, and B. Dieny, Influence of thermal annealing on the perpendicular magnetic anisotropy of Pt/Co/AlO$_x$ trilayers, Phys. Rev. B **79**, 024423 (2009).

[46] S. Ikeda, K. Miura, H. Yamamoto, K. Mizunuma, H. D. Gan, M. Endo, S. Kanai, J. Hayakawa, F. Matsukura, and H. Ohno, A perpendicular-anisotropy CoFeB-MgO magnetic tunnel junction, Nat. Mater. **9**, 721 (2010).

[47] C.-H. Lambert, A. Rajanikanth, T. Hauet, S. Mangin, E. E. Fullerton, and S. Andrieu, Quantifying perpendicular magnetic anisotropy at the Fe-MgO(001) interface, Appl. Phys. Lett. **102**, 122410 (2013).

[48] H. X. Yang, M. Chshiev, B. Dieny, J. H. Lee, A. Manchon, and K. H. Shin, First-principles investigation of the very large perpendicular magnetic anisotropy at Fe|MgO and Co|MgO interfaces, Phys. Rev. B **84**, 054401 (2011).

[49] T. Saito, T. Katayama, T. Ishikawa, M. Yamamoto, D. Asakura, T. Koide, Y. Miura, and M. Shirai, Interface structure of half-metallic Heusler alloy Co$_2$MnSi thin films facing an MgO tunnel barrier determined by x-ray magnetic circular dichroism, Phys. Rev. B **81**, 144417 (2010).

[50] S. Andrieu, A. Neggache, T. Hauet, T. Devolder, A. Hallal, M. Chshiev, A. M. Bataille, P. Le Fèrve, and F. Bertran, Direct evidence for minority spin gap in the Co$_2$MnSi Heusler compound, Phys. Rev. B **93**, 094417 (2016).